Thermodynamic curvature for attractive and repulsive intermolecular forces

Helge-Otmar May
University of Applied Sciences, Darmstadt, Germany, D-64295

Peter Mausbach
Cologne University of Applied Sciences, Cologne, Germany, D-50679

George Ruppeiner
Division of Natural Sciences, New College of Florida, Sarasota, Florida, USA
(Received 16 May 2013; published 17 September 2013)

The thermodynamic curvature scalar R for the Lennard-Jones system is evaluated in phase space, including vapor, liquid, and solid state. We paid special attention to the investigation of R along vapor-liquid, liquid-solid, and vapor-solid equilibria. Because R is a measure of interaction strength, we traced out the line $R = 0$ dividing the phase space into regions with effectively attractive ($R < 0$) or repulsive ($R > 0$) interactions. Furthermore, we analyzed the dependence of R on the strength of attraction applying a perturbation ansatz proposed by Weeks-Chandler-Anderson. Our results show clearly a transition from $R > 0$ (for poorly repulsive interaction) to $R < 0$ when loading attraction in the intermolecular potential.

DOI: 10.1103/PhysRevE.88.032123 PACS number(s): 51.30.+i, 61.20.−p, 05.70.−a, 64.10.+h

I. INTRODUCTION

The use of differential geometry in thermodynamics has a long and successful tradition [1–5]. It has been shown that fundamentally new results can be obtained when Riemannian geometry is introduced in equilibrium thermodynamics [6–8]. The Riemannian curvature scalar R is of special interest. R is calculated from the coefficients g_{ij} of the metric tensor given by derivatives of macroscopic state variables and defining a thermodynamic line element (see Appendix). This line element can be considered as a distance between two thermodynamic state points. R is a measure of interaction strength [9] where the sign of R specifies whether intermolecular interactions are effectively attractive ($R < 0$) or repulsive ($R > 0$) in the curvature sign convention of Weinberg [1]. Moreover, the magnitude $|R|$ of the invariant R can be interpreted as a measure of the size of mesoscopic organized structures in a fluid.

In a recent study, Ruppeiner [10] discusses the principal behavior of R in five different phase space regions: (1) in the vapor phase, (2) the compact liquid phase, (3) near the critical point (CP), (4) in the asymptotic CP regime, and (5) in the solid state. Additionally, Ruppeiner [10] evaluated R along the vapor-liquid coexisting line from the CP to the triple point (TP) for numerous pure fluids using data from the NIST Chemistry WebBook [11]. These calculations mark an important step in understanding the behavior of R for pure fluids. However, a verification of the mesoscopic fluid concept characterized by the thermodynamic curvature R for the complete phase space including vapor-liquid, liquid-solid, and vapor-solid equilibria would be desirable. Furthermore, a detailed analysis of the influence of intermolecular attraction and repulsion on the curvature R would certainly extend the understanding of Riemannian geometry of thermodynamics.

Therefore, the aim of our study is to fill this gap. We apply the ideas of the mesoscopic fluid concept to the very frequently discussed Lennard-Jones (LJ) system. Based on realistic multiparameter equations of state (EOS) for a LJ-system, we analyze the state-point-dependent behavior of R. We used the modified Benedict-Webb-Rubin (MBWR) EOS of Johnson *et al*. [12] to calculate the Helmholtz free energy of the LJ system in the fluid phase, because this EOS is the basis for a widely accepted EOS describing the thermodynamics of the face-centered cubic solid developed from van der Hoef [13,14]. An accuracy discussion for the MBWR EOS is already given in the original paper of Johnson *et al*. [12]. But it is not sufficient to examine the quality of an EOS by comparing only pressure and energy values; usually these parameters are fairly well represented by a multiparameter high-quality EOS. In Ref. [15], a comparison of different high-quality EOS including the MBWR EOS is given where fluid properties like thermodynamic response functions are calculated from these EOS and are compared with NVEPG ensemble simulation results. This new NVEPG ensemble simulation method allows a direct calculation of thermodynamic derivatives. In Sec. V of this paper, we use the original MBWR EOS and a revised MBWR EOS [8], to calculate the important $R = 0$ line in order to check the sensitivity to a change of the EOS. The results for both EOS are very similar.

In this study, we first investigate the dependence of R on the intermolecular strength. For this purpose, we use a separation ansatz proposed by Weeks-Chandler-Anderson (WCA) [16], where the intermolecular potential is separated into a short-range repulsive and a long-range attractive component. The latter is treated as a perturbation. This treatment allows us to load attraction continuously to the repulsive part of the potential. Second, we use this separation ansatz to map out the vapor-liquid coexisting line depending on the strength of interaction. Here, we apply the R-crossing method [7]. Additionally, we numerically estimate the critical behavior of R and compare it with a consideration given by Ruppeiner [10]. In the remainder of the paper, we evaluate the behavior of R for the complete phase space where we concentrate on the full LJ potential only. We investigate the thermodynamic curvature scalar R in the solid state by using an EOS developed by

van der Hoef [13,14] for the face-centered cubic-LJ solid. In the following part, we study the behavior of R along liquid-solid and vapor-solid equilibria. Additionally, we locate the line $R = 0$ in phase space, which is close to the liquid-solid first-order phase transition. The line $R = 0$ indicates a change in interaction from effectively attractive to repulsive. In the Appendix, we describe how the thermodynamic curvature scalar R can be calculated from any EOS given in density-temperature coordinates.

We add that an early attempt to relate the correlation function to fluctuating thermodynamic quantities described by a thermodynamic correlation matrix was by Green [17].

II. DEPENDENCE OF R ON INTERMOLECULAR FORCES IN THE FLUID PHASE

One of the key statements in Riemannian geometry of thermodynamics is that the thermodynamic curvature scalar R measures intermolecular interaction and the sign of R indicates whether the interaction is effectively attractive or repulsive [9]. It is expected that a fluid with LJ-type interaction is dominated by attractive forces with negative R and that R diverges to $-\infty$ at the critical point [10].

Nevertheless, for a LJ-type fluid, a region of small positive R is expected near the fluid-solid transition, indicating a change to effectively repulsive interaction. However, a systematic study of the influence of the attractive forces on the behavior of the thermodynamic curvature R has not been performed until now. In order to investigate this role, we varied the intensity of these forces and we used a separation ansatz of the LJ potential proposed by WCA [16].

The Lennard-Jones potential is

$$U_{\mathrm{LJ}}(r) = 4\varepsilon\left[\left(\frac{\sigma}{r}\right)^{12} - \left(\frac{\sigma}{r}\right)^{6}\right]. \tag{1}$$

Here, ϵ is the LJ well depth, σ is the LJ atomic diameter, and r is the distance between two particles.

In the following, we use reduced quantities for the distance r with $r^* = r/\sigma$, the time τ with $\tau^* = \tau\sqrt{\varepsilon/m\sigma^2}$ (m is the mass of a particle), the temperature T with $T^* = k_B T/\varepsilon$ (k_B is Boltzmann's constant), the energy E with $E^* = E/\varepsilon$, the density ρ with $\rho^* = \rho\sigma^3$ ($\rho = N/V$ is the number density for N particles in the volume V), and the pressure p with $p^* = p\sigma^3/\varepsilon$. For the Riemannian thermodynamic curvature, we get $R^* = R/\sigma^3$ (compare Appendix). All quantities quoted in this work are in these reduced terms and the asterisk superscript will be omitted in the rest of the paper.

The full intermolecular potential U is decomposed into a reference part U_0 and a perturbation part U_P:

$$\begin{aligned} U(r) &= U_0(r) + \lambda\, U_P(r) \\ U_0(r) &= \begin{cases} U_{\mathrm{LJ}}(r) + 1, & r \leqslant r_m \\ 0, & r > r_m \end{cases} \\ U_P(r) &= \begin{cases} -1, & r \leqslant r_m \\ U_{\mathrm{LJ}}(r), & r > r_m \end{cases}, \end{aligned} \tag{2}$$

where $r_m = 2^{1/6}$. The reference part U_0 describes short-range repulsive forces and the perturbation part U_P includes all the long-range attractive forces. λ is a coupling parameter that loads the effect of attraction by varying continuously from

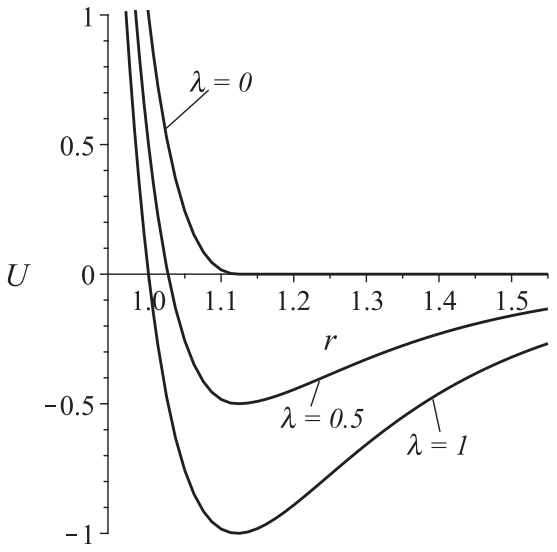

FIG. 1. Intermolecular potential $U(r) = U_0(r) + \lambda U_P(r)$ for $\lambda = 0$, 0.5, and 1 (from top to bottom).

$\lambda = 0$ (poorly repulsive WCA potential [16]) to $\lambda = 1$ (full LJ potential). In our analysis, we considered three values of λ ($\lambda = 0$, 0.5, and 1; see Fig. 1).

To investigate the Riemannian curvature scalar R according to the formulas given in the Appendix, the Helmholtz free energy (HFE) has to be calculated from an EOS. Cuadros *et al.* [18] developed a parametric representation for the excess HFE depending on the thermodynamic state point and the coupling parameter λ according to Eq. (2). However, these relatively simple polynomial ansatz functions used there are not appropriate for calculating the curvature R where higher order derivatives of the ansatz functions are used. Because of the lack of one adequate multiparameter EOS for each value of λ, we used different EOS for each case.

A. The case $\lambda = 0$ (poorly repulsive WCA potential-EOS)

A WCA-EOS for $\lambda = 0$ is obtained from a variation of the classical Carnahan-Starling [19] equation of the compressibility factor $Z = p/(\rho T)$ in terms of the packing fraction of hard spheres ($y = \pi\rho\sigma_{\mathrm{HS}}^3/6$):

$$Z = \frac{1 + y + ay^2 - by^3}{(1-y)^3}\,. \tag{3}$$

In the original Carnahan-Starling equation, the adjustable parameters are $a = b = 1$. A WCA-EOS is obtained by substituting the hard-sphere diameter σ_{HS} with a temperature-dependent formula. For this purpose, various approaches exist [20,21]. We used the equations of Heyes and Okumura [22] with

$$\sigma_{\mathrm{HS}} = \frac{2^{1/6}}{(1+\sqrt{T})^{1/6}} \tag{4}$$

and $a = 3.597, b = 5.836$ in order to calculate the HFE because the Heyes and Okumura formulas yield good agreement for the compressibility factors at all temperatures.

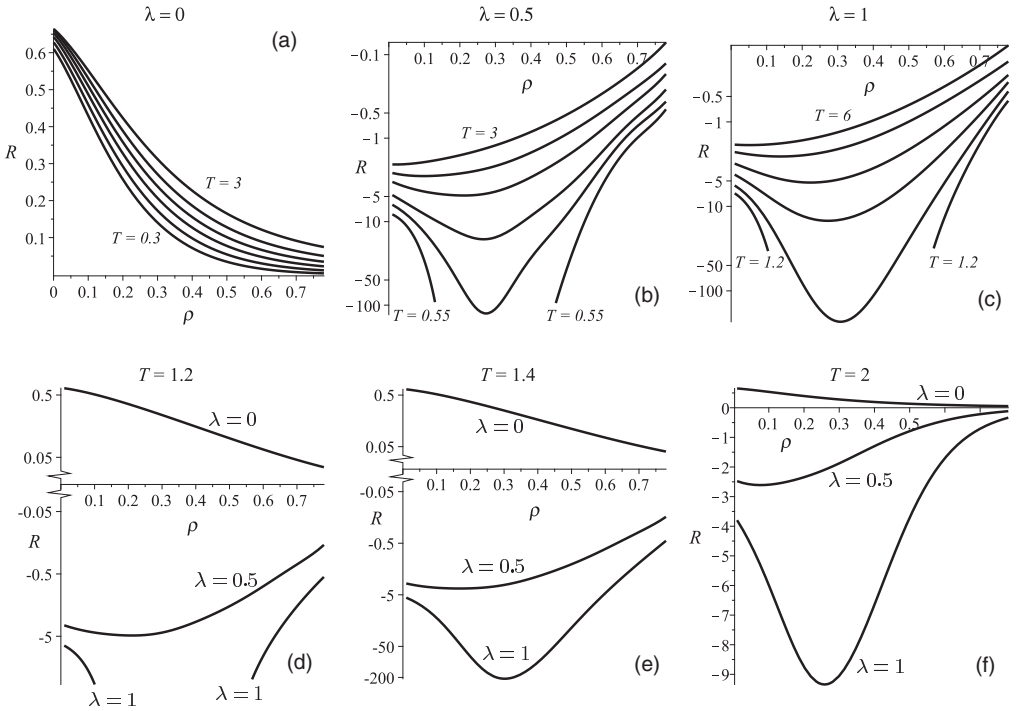

FIG. 2. Density dependence of thermodynamic curvature R at different constant temperatures for coupling parameters $\lambda = 0$, 0.5, and 1. (a) Isotherms of R for $\lambda = 0$ and $T = 0.3$, 0.5, 0.8, 1.2, 1.8, and 3.0 (bottom to top); (b) isotherms of R for $\lambda = 0.5$ and $T = 0.55$, 0.65, 0.8, 1.2, 1.8, and 3.0 (bottom to top); (c) isotherms of R for $\lambda = 1.0$ and $T = 1.2$, 1.4, 1.8, 2.5, 4.0, and 6.0 (bottom to top); (d) isotherms of R for $T = 1.2$; (e) for $T = 1.4$; (f) for $T = 2.0$. In (d), (e), and (f), curves are shown for $\lambda = 0$, 0.5, and 1.0 from top to bottom. All state points shown in this figure belong to the fluid phase; for $\lambda = 0$ compare Ref. [24]. The critical temperatures in reduced units are $T_c = 0$ for $\lambda = 0$, $T_c = 0.598$ for $\lambda = 0.5$, and $T_c = 1.313$ for $\lambda = 1$.

B. The case $\lambda = 0.5$ (MBWR/WCA05-EOS)

To our knowledge, no proper EOS exists in literature for $\lambda = 0.5$. Therefore, we had to develop our own EOS, where an ansatz of a modified Benedict-Webb-Rubin (MBWR) [12,23] type expression was used. We will use the abbreviation MBWR/WCA05-EOS for the case $\lambda = 0.5$ in our study. We performed molecular-dynamics (MD) simulations in a NVE ensemble on a homogenous fluid of 1024 particles. The simulations covered densities ranging from $\rho = 0.05$ to 0.8 and temperatures ranging from $T = 0.4$ to 3.0 with more than 300 thermodynamic state points. The equations of motion were integrated with a time step of $\tau = 0.003$. For each state point simulation trajectories were run for 5×10^4 time steps to equilibrate the system. Periods of 4×10^5 time steps were used to accumulate the average values of the thermodynamic state variables. The cutoff radius for the potential was $4.0\,\sigma$. The MBWR/WCA05-EOS for the pressure p as function of density ρ and temperature T contains 33 adjustable parameters, which are fitted with our MD-simulation data. The fitting procedure is similar to the description elsewhere [8] and shall therefore not be repeated here.

C. The case $\lambda = 1.0$ (MBWR EOS)

For $\lambda = 1.0$, the interaction potential is a full LJ potential. We use the MBWR EOS of Johnson *et al.* [12] to calculate the HFE in the fluid phase because this MBWR EOS is the basis for the analysis at the solid-liquid transition (see Sec. IV).

D. Comparison of the three cases

In Fig. 2, the density dependence of R at constant temperatures for different coupling parameters λ is shown. In Fig. 2(a) the curvature R is shown for $\lambda = 0$ (poorly repulsive WCA EOS) for temperatures $T = 3.0$, 1.8, 1.2, 0.8, 0.5, and 0.3 (from top to bottom). The thermodynamic curvature R is positive for the densities and temperatures in the fluid phase shown in the figure and R decreases monotonically with increasing density and decreasing temperature. This behavior confirms the physical interpretation [10] that $R > 0$ indicates effectively repulsive interactions. The behavior of R changes drastically when attraction is loaded in the intermolecular potential causing a first-order vapor-liquid transition associated with a critical point. Figure 2(b) shows the curvature calculated from the MBWR/WCA05 EOS ($\lambda = 0.5$) for temperatures $T = 3.0$, 1.8, 1.2, 0.8, 0.65, and 0.55 (from top to bottom), whereas in Fig. 2(c) the curvature for the MBWR EOS ($\lambda = 1.0$) is shown for temperatures $T = 6.0$, 4.0, 2.5, 1.8, 1.4, and 1.2 (from top to bottom). The curves are broken at the intersection of the vapor-liquid coexistence line.

The critical temperatures in reduced units are $T_c = 0$ for $\lambda = 0$, $T_c = 0.598$ for $\lambda = 0.5$, and $T_c = 1.313$ for $\lambda = 1$. The critical temperature for $\lambda = 0.5$ was calculated from the fit using the conditions $\partial p/\partial\rho|_{\rho_c,T_c} = 0$ and $\partial^2 p/\partial\rho^2|_{\rho_c,T_c} = 0$.

For $\lambda = 0.5$ and $\lambda = 1$ [Figs. 2(b) and 2(c)], the interaction is effectively attractive causing negative curvature R in the whole density region shown in Fig. 2. The curvature strongly decreases toward the critical point and becomes singular at

the critical point. The influence of λ on R is shown for three constant temperatures $T = 1.2$ [Fig. 2(d)], $T = 1.4$ [Fig. 2(e)], and $T = 2$ [Fig. 2(f)]. Each figure shows the curvature R for $\lambda = 0, 0.5$, and 1.0 (from top to bottom). A transition from $R > 0$ to $R < 0$ with loading attraction is obvious for each state point confirming again the physical interpretation of R [10].

We conclude this section with a comment about the limiting low-density behavior of R shown in Fig. 2. An exact calculation [3] shows that $R = 0$ for the ideal gas, a result which nicely suggests a connection between R and intermolecular interactions. However, we should be careful not to over-interpret this result in the context of Fig. 2, where R does not go to zero in the limit $\rho \to 0$. There are two points to consider. First, in this paper, R was not worked out with the ideal gas law, but for a gas with interactions, albeit weakening as the density gets smaller. Second, Ruppeiner [10] has articulated a "low $|R|$ limit," $|R| \ll \rho^{-1}$ as indicating a volume regime where physical interpretations of R come into question. This limit marks the situation where the volume defined by $|R|$ is much less than the typical volume in the voids between adjacent molecules. We expect thermodynamics to have some difficulties at volumes this small. The ideal gas corresponds to a special case, since for it *any* finite R is in the low $|R|$ limit, and the limiting low-density values for R in Fig. 2 cannot be interpreted strictly in terms of organized structure sizes. However, the major results in this paper are mostly above the low $|R|$ limit, and the physical picture developed for R here should be a good one. Cases where we have come close to the low $|R|$ limit should be clear.

III. BEHAVIOR AT VAPOR-LIQUID EQUILIBRIA AND AT THE CRITICAL POINT

For a van der Waals (vdW) fluid, Ruppeiner *et al.* [7] showed for the first time how the vapor-liquid coexisting line can be calculated by the so-called R-crossing method. In the following, this approach was applied to the more realistic LJ fluid [8]. The dependence of the course of the vapor-liquid coexisting line on the intensity of attractive forces has not been studied until now and is the purpose of this section.

In Fig. 3, we present the vapor-liquid coexistence line in the (ρ,T) projection for $\lambda = 0.5$ and 1. We constructed the vapor-liquid coexistence line by using standard thermodynamic requirements of equality for the pressure and the Gibbs free energy at a given temperature (continuous lines). Additionally, we calculated the coexistence line using the R-crossing method [7,8] where the equality of the thermodynamic scalar curvature R is required in the two coexisting phases (solid circles). The overall agreement for both methods is very good, similar to Ref. [8]. Only for temperatures $T < 0.52$, the coexistence lines for $\lambda = 0.5$ of the two methods differ on the vapor site. Obviously, the correlation volume is not large enough to encompass a number of particles adequate for a thermodynamic approach, because the length scale at state points in this region is below the low $|R|$ limit [7,10] where the R-crossing method loses its applicability. The coexistence curve for $\lambda = 0.5$ is enclosed by the $\lambda = 1$ curve. For $\lambda = 0$ the critical point moves to $T = 0$ and the vapor-liquid coexistence line disappears.

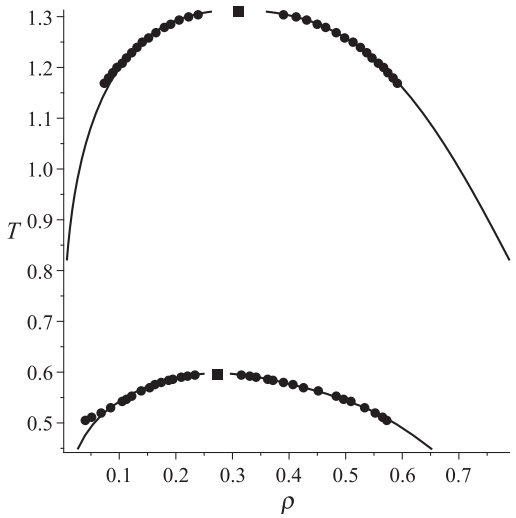

FIG. 3. Vapor-liquid coexistence line in the ρ-T projection for $\lambda = 0.5$ (lower) and $\lambda = 1.0$ (upper curve). The coexisting curves are calculated from the equality for the pressure and Gibbs free energy at a given temperature (continuous lines) as well as the R-crossing method (solid circles) in the two phases. The critical point is marked by a solid square.

As stated before, the thermodynamic curvature diverges to $-\infty$ at the critical point. In Fig. 4, the asymptotic behavior of R near the critical point for $\lambda = 0.5$ and for $\lambda = 1$ is shown. In this region, the asymptotic behavior of R was analyzed by Ruppeiner [10]. R, calculated along the coexisting curve, has the same critical exponent as ξ^3, because the relation $|R| \sim \xi^3$ is valid [6] between R and the volume ξ^3 of the correlation length ξ. It was shown [10] that R diverges with exponent $a = 2 - \alpha$, where R can be described by

$$R = -C \left(\frac{T_c}{T_c - T} \right)^a \tag{5}$$

along the coexistence curve near the critical point. Because the MBWR EOS is classical [12], the critical exponent of the specific heat is $\alpha = 0$. Based on the MBWR EOS, the curvature R should diverge with $a = 2$. The same is true for the vdW EOS. We calculated the exponent for the results shown in Fig. 4. The value depends on the distance from the critical point. When fitting the results for $\lambda = 1$ between $\Delta T = 0.03$ and 0.003 (ΔT is the temperature distance from the critical point), we found $a = 2.01$; for ΔT between 10^{-5} and 6×10^{-7}, we found $a = 2.000005$. Something similar is valid for $\lambda = 0.5$. Additionally, we also calculated the exponent using the vdW EOS with a value of a = 2.0 when reaching the critical temperature, too.

IV. THE THERMODYNAMIC SCALAR CURVATURE R IN THE SOLID STATE

For the rest of the paper we concentrate on the full LJ potential ($\lambda = 1$) in order to study the interplay between repulsive and attractive intermolecular forces for this potential at different transition lines as well as in the solid state.

The highly organized solid state is held up by the repulsive part of intermolecular interactions for which we expect $R > 0$

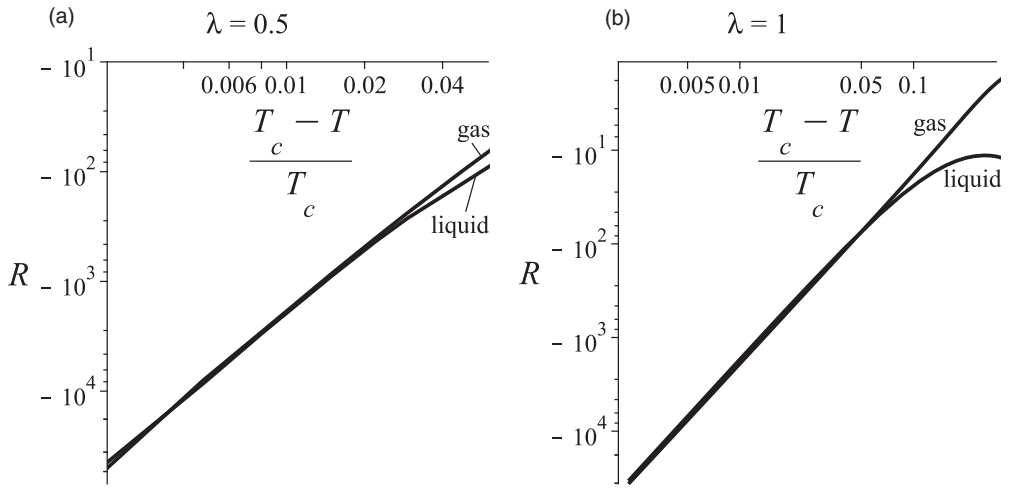

FIG. 4. Thermodynamic curvature R for the coexisting vapor and liquid phases versus $(T_c - T)/T_c$ near the critical temperature T_c for (a) $\lambda = 0.5$ and (b) $\lambda = 1$.

[10]. A proof of this expectation was not given so far. A widely accepted EOS that describes the thermodynamics of the fcc-LJ solid is the EOS developed from van der Hoef (vdH-EOS) [14]. van der Hoef determined an expression for the absolute HFE from MD simulation data. The HFE at an arbitrary state point in the solid phase was obtained by integrating over density and temperature from the triple point. Therefore, triple point data and an EOS for the liquid are required in this approach for which van der Hoef applied the MBWR EOS [12]. It is of interest to investigate the scalar curvature R in the solid state obtained from the vdH-EOS in connection with our analysis in the liquid phase. van der Hoef stated that the fitting data for densities were ranging from around $\rho = 0.94$ to 1.2 and the results were most accurate in the temperature range from $T = 0.3$ to 2.

In Fig. 5, we present the density and temperature dependence of the curvature R in the solid state starting around the freezing transition. In Fig. 5(a), we present the density dependence of R in the vicinity of the liquid-solid transition for constant temperatures $T = 2.0$, 1.8, and 1.5 on the liquid and the solid side. The gradients of R are much higher in the liquid phase. Figure 5(b) shows the density dependence of the scalar curvature R along different constant lower temperatures ($T = 0.35$, 0.45, 0.55, 0.65, and 0.75). Figure 5(c) shows the temperature dependence of R along different constant densities ($\rho = 1.0$, 1.1, and 1.2). The curves start at $T = 0.3$ and are terminated at the melting point, respectively. For $\rho = 1$, the line is continued in the liquid region until $T = 2$. For $\rho = 1.1$ and 1.2, the liquid region starts at $T > 2$. The results from Fig. 5 confirm the prediction that R is positive in the solid state and they show that R mostly increases with increasing density.

V. THE LINE $R = 0$ AND THE BEHAVIOR OF R AT LIQUID-SOLID AND VAPOR-SOLID EQUILIBRIA

In the previous chapters we have shown that R is mainly negative in the liquid phase, indicating effectively attractive interaction, and R is positive everywhere in the solid state, indicating effectively repulsive interaction. Consequently, there must exist a line with $R = 0$, and this line should indicate a change in interaction.

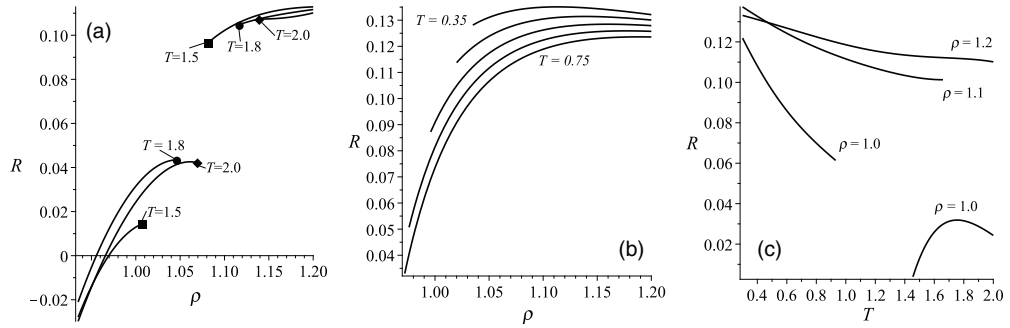

FIG. 5. (a) Density dependence of the scalar curvature R along different constant temperatures ($T = 1.5$, 1.8, and 2.0) in the vicinity of the liquid-solid phase transition. The curves on the liquid and the solid site are terminated at the freezing and the melting point, respectively. (b) Density dependence of the scalar curvature R along different constant lower temperatures ($T = 0.35$, 0.45, 0.55, 0.65, and 0.75). (c) Temperature dependence of the scalar curvature R along different constant densities ($\rho = 1.0$, 1.1, and 1.2). The curves start at $T = 0.3$ and are terminated at the melting point, respectively. For $\rho = 1$ the line is continued in the liquid region until $T = 2$. For $\rho = 1.1$ and 1.2, the liquid region starts at $T > 2$.

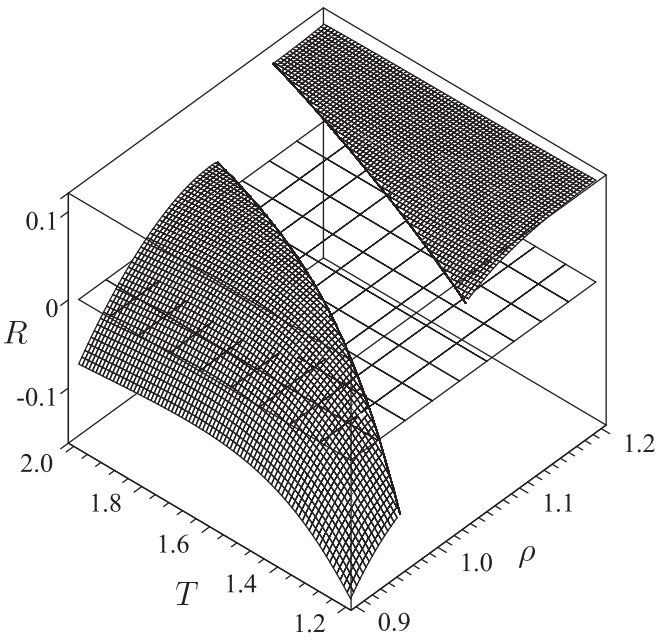

FIG. 6. Surface of thermodynamic curvature scalar R depending on density and temperature close to the liquid-solid phase transition.

In Fig. 6, we present the surface of curvature R depending on density (ranging from $\rho = 0.9$ to 1.2) and temperature (ranging from $T = 1.2$ to 2.0) at the liquid-solid transition as well as in the solid and the liquid phase. In the liquid phase, R is calculated from the MBWR EOS [12], whereas in the solid state the vdH EOS [14] was used. It is obvious that the surface R on the liquid site intersects the plane $R = 0$ close to the liquid-solid phase transition. Along the freezing line, R changes the sign at about $T = 1.44$ from negative to positive.

In Fig. 7(a), this intersection curve is mapped out in the density-temperature projection. Additionally, the vapor-liquid coexisting line (BCT) with its corresponding critical point (C) and the liquid-solid (TD and FE and continuation for $T > 2$) and the vapor-solid (AB and FG) coexisting lines are shown. These lines are constructed for $0.3 < T < 2$ from the condition that pressure and Gibbs free energy achieve equal values. Because the MBWR EOS is only valid for $T > 0.7$, an equation of state with the second virial coefficient was used for the vapor phase along AB. For $T > 2$, the lines are drawn from analytical expressions ([14], compare Agrawal and Kofke [25]).

Because higher-order derivatives have to be calculated from the EOS for the construction of the thermodynamic curvature R, the results could be very sensitive to a change of the EOS [15]. Therefore, it makes sense to compare the results for different EOS. For the full LJ potential, a new revised MBWR-EOS was published recently [8]. The new EOS was developed because newer simulation data of Meier [26] were used by different researchers. To distinguish between both equations we will use the abbreviation MBWR/2012 for the new revised EOS. Besides the $R = 0$ curve for the MBWR EOS of Johnson *et al.* (solid line in Fig. 7), we also show the intersection curve for the MBWR/2012 EOS (dashed line in Fig. 7). Both calculations show a similar behavior. The curves run at a roughly constant density of $\rho \approx 0.95$ before a sharp turn toward the solid state occurs at approximately $T \approx 1.5$. Having in mind that liquid Argon is well represented by LJ-type interactions, it is of interest to note that no $R = 0$ point was found along the vapor-liquid coexisting line according to our results. Nor was such a point found in real Argon by Ruppeiner [10] done in the context of fits to fluid data from the NIST Chemistry WebBook.

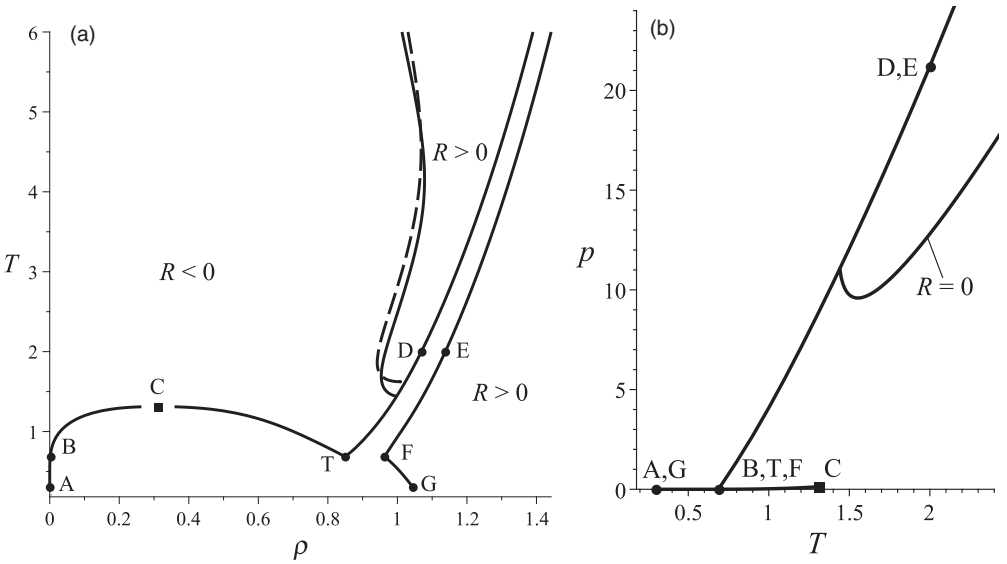

FIG. 7. Phase diagram for $\lambda = 1$: (a) Lines where $R = 0$ in the density-temperature projection as well as the vapor-liquid (BCT) coextisting line with the corresponding critical point (solid square, C) and the liquid-solid (TD and FE and continuation for $T > 2$) and the vapor-solid (AB and FG) coexisting lines. The lines where $R = 0$ are calculated from the original MBWR-EOS of Johnson *et al.* [12] (solid line) and from the MBWR/2012 EOS [8] (dashed line). (b) Phase diagram in the temperature-pressure projection: Here, the $R = 0$ line only for the MBWR EOS of Johnson *et al.* is drawn.

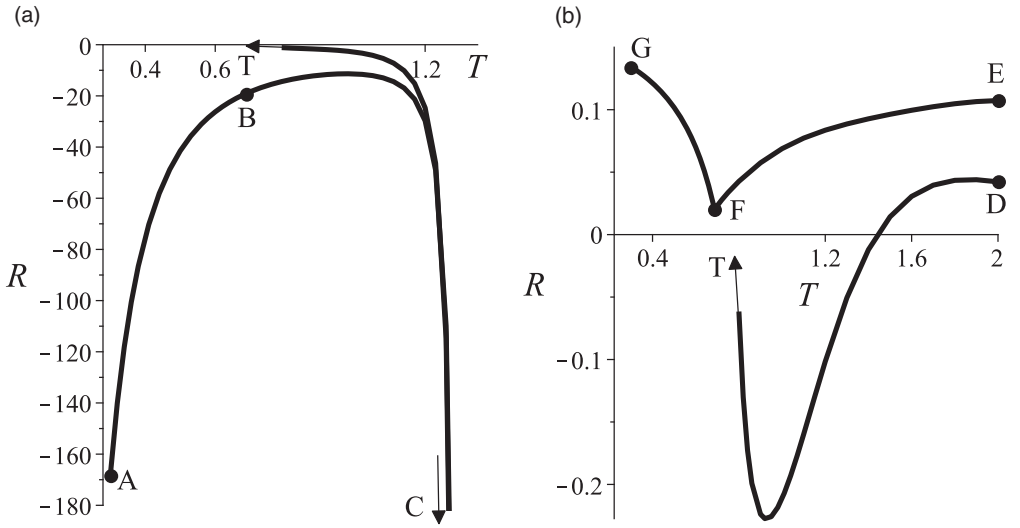

FIG. 8. (a) Thermodynamic curvature along the vapor-liquid line (BC and CT) and the low-density vapor-solid line (AB) as a function of the temperature. The points A, B, C, and T are shown in the (ρ-T) projection of Fig. 7. (b) Thermodynamic curvature along the vapor-solid and liquid-solid line as a function of the temperature. The points D, E, F, G, and T are shown in the (ρ-T) projection of Fig. 7.

In Fig. 7(b), the temperature-pressure projection of the phase diagram is shown. Here, the curve with $R = 0$ is drawn only for the MBWR EOS of Johnson *et al*. Starting from the solid-liquid line, the curve corresponds to a decrease in pressure with temperature increase before passing through a minimum, then the pressure is increasing with temperature increase.

It is natural to ask whether the $R = 0$ curve might coincide with the well-known Fisher-Widom line [27], because this curve also marks a transition from attractive to repulsive interaction. However, the precise correspondence between the Fisher-Widom line and the line $R = 0$ remains an open interesting research issue.

In Fig. 8(a), R is drawn along the vapor-liquid (BC and CT) and the low-density vapor-solid coexisting line (AB). The two lines, which start from the critical point C, represent the vapor site (ABC with $\rho < \rho_c$) and the liquid site (CT with $\rho > \rho_c$) of the corresponding coexisting lines. The vapor branch of the vapor-solid coexisting line starts at a temperature of $T = 0.3$ (point A), from where the vdH EOS is valid in the corresponding solid state, too. The curvature R diverges to $-\infty$ at the critical point (C) and decreases strongly toward point A as the molar volume increases in the vapor phase. Figure 8(b) shows the freezing (TD) and the melting line (FE) at the liquid-solid transition as well as the solid branch of the vapor-solid coexisting line (FG). The curvature R changes the sign along the freezing line (TD) at about $T \approx 1.44$, as we have discussed before.

The MBWR EOS of Johnson *et al*. (but also the MBWR/2012 EOS) is fitted by using simulation data down to temperatures of $T = 0.7$. Extrapolating the results for both equations to the triple point with $T < 0.7$ leads to different results and causes uncertainties in the prediction of R. Therefore, the lines are stopped before reaching point T (indicated by an arrow).

VI. CONCLUSION

In this study, we analyzed in detail the dependence of the thermodynamic curvature scalar R on the intermolecular strength by using a separation ansatz proposed by Weeks-Chandler-Anderson. This separation ansatz allows an investigation of the behavior of R by changing the interaction continuously from the poorly repulsive WCA potential to the full LJ potential. The analysis is based on different multiparameter EOS. For intermediate attraction ($\lambda = 0.5$), we developed a MBWR-EOS based on a set of new MD simulation data. The results show clearly a transition from $R > 0$ for poorly repulsive interaction to $R < 0$ when loading attraction.

Furthermore, we traced out the vapor-liquid coexisting lines depending on the interaction strength by applying standard thermodynamic requirements and the new R-crossing method. We obtained good agreement between both methods in the limits of their applicability. We also confirmed numerically theoretical predictions for critical point properties of R and find that for the classical MBWR-EOS the curvature R diverges with an exponent of 2 at the CP.

In the following, we explored the state point dependent behavior of R in the whole phase space for a full LJ potential. Based on the vdH-EOS for an face-centered-cubic-LJ-solid we could show that the curvature R is positive, as expected, in the whole density-temperature range for which the vdH-EOS was constructed.

Special attention was paid to the calculation of R along liquid-solid and vapor-solid equilibria. R is positive at the solid side along both liquid-solid and vapor-solid line according to the statement before. On the vapor side of the vapor-solid coexisting line, R is negative and decreases strongly when temperature decreases and the molar volume increases. On the freezing line at the liquid-solid transition, R starts with $R < 0$ for temperatures slightly above the TP-temperature and

changes the sign at about $T \approx 1.44$. This is the starting point of the line $R = 0$, which indicates a change in interaction. We mapped out the line $R = 0$ in the liquid region, which is close to the liquid-solid transition.

In summary, we believe that the investigations of our study offer new and interesting insights into the behavior of the curvature R for the thermodynamics of fluid systems. Our study is part of a larger effort at classifying R in all thermodynamic systems, including fluids, solids, and spin systems. In addition, these findings may extend to black-hole thermodynamics, where there is absolutely no consensus about the correct microscopic Hamiltonian. The calculation of R offers one of the few direct methods available for probing microscopic elements of black holes; see Åman *et al.* [5] for review. But attempts to make sense of the black-hole behavior by these means requires an excellent understanding of R in ordinary thermodynamics [29]. The study here extends this effort.

APPENDIX: CALCULATION OF R

The thermodynamic line element $d\ell$ is given by the thermodynamic entropy information metric [10]:

$$d\ell^2 = \sum_{i,j} g_{ij} dq^i dq^j. \tag{A1}$$

$d\ell^2$ is an invariant in the thermodynamic parameters q^i and the coefficients g_{ij} are the components of the metric tensor. For a one-component fluid there are two independent state variables q^1 and q^2 and the Riemannian curvature is calculated from ([6,10,28])

$$R = -\frac{1}{\sqrt{g}}\left[\frac{\partial}{\partial q^1}\left(\frac{g_{12}}{g_{11}\sqrt{g}}\frac{\partial g_{11}}{\partial q^2} - \frac{1}{\sqrt{g}}\frac{\partial g_{22}}{\partial q^1}\right) + \frac{\partial}{\partial q^2}\left(\frac{2}{\sqrt{g}}\frac{\partial g_{12}}{\partial q^1} - \frac{1}{\sqrt{g}}\frac{\partial g_{11}}{\partial q^2} - \frac{g_{12}}{g_{11}\sqrt{g}}\frac{\partial g_{11}}{\partial q^1}\right)\right], \tag{A2}$$

with

$$g = g_{11}\, g_{22} - g_{12}^2. \tag{A3}$$

By the rules of Riemannian geometry, the value of the curvature for any thermodynamic state is independent of the coordinate system. We choose ρ and T as independent variables and the basis of our analysis for R is the Helmholtz free energy $A(T,N,V)$. This quantity per volume is ([8,10])

$$f = \frac{A}{V}. \tag{A4}$$

f is associated with the specific free energy a by $f = \rho\, a$. (T, ρ) coordinates are orthogonal and the curvature R becomes

$$R = \frac{1}{\sqrt{g}}\left[\frac{\partial}{\partial T}\left(\frac{1}{\sqrt{g}}\frac{\partial g_{\rho\rho}}{\partial T}\right) + \frac{\partial}{\partial \rho}\left(\frac{1}{\sqrt{g}}\frac{\partial g_{TT}}{\partial \rho}\right)\right], \tag{A5}$$

with

$$g_{\rho\rho} = \frac{1}{T}\frac{\partial^2 f}{\partial \rho^2}, \quad g_{TT} = -\frac{1}{T}\frac{\partial^2 f}{\partial T^2}, \quad \text{and} \quad g = g_{TT}\, g_{\rho\rho}. \tag{A6}$$

In this formula, the specific free energy is calculated from the EOS, which was discussed in the previous sections.

[1] S. Weinberg, *Gravitation and Cosmology* (Wiley, New York, 1972).
[2] F. Weinhold, J. Phys. Chem. **63**, 2479 (1975).
[3] G. Ruppeiner, Phys. Rev. A **20**, 1608 (1979).
[4] P. Salamon and R. S. Berry, Phys. Rev. Lett. **51**, 1127 (1983).
[5] J. E. Åman, J. Bedford, D. Grumiller, N. Pidokrajt, and J. Ward, J. Phys.: Conf. Ser. **66**, 012007 (2007).
[6] G. Ruppeiner, Rev. Mod. Phys. **67**, 605 (1995); **68**, 313 (1996).
[7] G. Ruppeiner, A. Sahay, T. Sarkar, and G. Sengupta, Phys. Rev. E **86**, 052103 (2012).
[8] H.-O. May and P. Mausbach, Phys. Rev. E **85**, 031201 (2012); **86**, 059905(E) (2012).
[9] G. Ruppeiner, Am. J. Phys. **78**, 1170 (2010).
[10] G. Ruppeiner, Phys. Rev. E **86**, 021130 (2012).
[11] NIST Chemistry WebBook, http://webbook.nist.gov/chemistry/.
[12] J. K. Johnson, J. A. Zollweg, and K. E. Gubbins, Mol. Phys. **78**, 591 (1993).
[13] M. A. van der Hoef, J. Phys. Chem. **113**, 8142 (2000).
[14] M. A. van der Hoef, J. Phys. Chem. **117**, 5092 (2002).
[15] H.-O. May and P. Mausbach, AIP Conf. Proc. **1501**, 954 (2012).
[16] J. D. Weeks, D. Chandler, and H. C. Anderson, J. Chem. Phys. **54**, 5237 (1971).
[17] M. S. Green, J. Math. Phys. **9**, 875 (1968).
[18] F. Cuadros, W. Okrasinski, and A. Sanfeld, J. Chem. Phys. **104**, 5594 (1996).
[19] N. F. Carnahan and K. E. Starling, J. Chem. Phys. **51**, 635 (1969).
[20] L. Verlet and J. J. Weis, Phys. Rev. A **5**, 939 (1972).
[21] J. Kolafa and I. Nezbeda, Fluid Phase Equilib. **100**, 1 (1994).
[22] D. M. Heyes and H. Okumura, J. Chem. Phys. **124**, 164507 (2006).
[23] J. J. Nicolas, K. E. Gubbins, W. B. Streett, and D. J. Tildesley, Mol. Phys. **37**, 1429 (1979).
[24] A. Ahmed and R. J. Sadus, Phys. Rev. E **80**, 061101 (2009).
[25] R. Agrawal and D. A. Kofke, Mol. Phys. **85**, 43 (1995).
[26] K. Meier, Ph.D. thesis, University of the Federal Armed Forces, Hamburg, 2002.
[27] M. E. Fisher and B. Widom, J. Chem. Phys. **50**, 3756 (1969).
[28] I. S. Sokolnikoff, *Tensor Analysis* (Wiley, New York, 1951).
[29] G. Ruppeiner, J. Phys.: Conf. Ser. **410**, 012138 (2013).